UNIVERSITY OF
BATH

University of Bath

1   **_In situ_ extracting organic-bound calcium: a novel approach to mitigating organic fouling in**

2   **forward osmosis treating wastewater via gradient diffusion thin-films**

3   Ling Li[a], Xinhua Wang[a,*], Ming Xie[b], Zhiwei Wang[c], Xiufen Li [a,*], Yueping Ren[a]

4   [a] Jiangsu Key Laboratory of Anaerobic Biotechnology, School of Environmental and Civil

5   Engineering, Jiangnan University, Wuxi, P.R. China

6   [b] Institute for Sustainability and Innovation, College of Engineering and Science, Victoria University,

7   Melbourne, Australia

8   [c] State Key Laboratory of Pollution Control and Resource Reuse, School of Environmental Science

9   and Engineering, Tongji University, Shanghai, P.R. China

10

11   [*]Corresponding author. E-mail: xhwang@jiangnan.edu.cn (X. Wang), xfli@jiangnan.edu.cn (X.

12   Li); Tel: +86-510-85326516.

13

14

15

16

17

18

19

20

21

22

23   **Abstract**

24   Forward osmosis (FO) has gained increasing interests in wastewater treatment and reclamation.

25   However, membrane fouling has become one major obstacle hindering FO application. A novel

26   mitigation approach for FO membrane fouling via *in situ* extracting Ca^{2+} binding with the organic

27   foulants using the gradient diffusion thin-films (DGT) was proposed in this study. The DGT could

28   effectively adsorb the Ca^{2+} binding with the sodium alginate via the chelation of the Chelex

29   functional groups, and its adsorption amount of Ca^{2+} correspondingly increased as a function of the

30   Ca^{2+} concentration in the feed solution. Owing to the extraction of Ca^{2+} from the fouling layer by

31   the DGT, the FO membrane fouling was effectively mitigated evident by significant enhancement

32   of water flux, and at the same time, foulants became easily removed by physical cleaning. The

33   alleviation of FO membrane fouling by the DGT could be attributed to the fact that the structure of

34   the fouling layer became more porous and looser after *in situ* removing Ca^{2+} from the alginate-Ca^{2+}

35   gel networks. The feasibility of fouling control strategy via *in situ* removing Ca^{2+} binding with the

36   foulants in the fouling layer was demonstrated, which provides new insights into fouling control

37   mechanisms during FO treating wastewater.

38   **Keywords**: forward osmosis, membrane fouling, organic foulants, calcium, gradient diffusion thin-

39   films, wastewater treatment

40

41

42

43

44

1. Introduction

Forward osmosis (FO) process has raised increasing attentions as a promising technology for wastewater treatment and reclamation (Liu and Mi, 2012; Zhao et al., 2012; Lutchmiah et al., 2014). FO process utilizes osmotic pressure gradient as driving force to extract water molecule from the feed solution (FS) through the FO membrane to the draw solution (DS). Compared to the pressure-driven membrane processes including reverse osmosis (RO) and nanofiltration (NF), the osmotic pressure-driven FO process has several advantages such as lower energy consumption (if no need to regenerate the draw solution), higher water recovery, and superior water flux stability against fouling (McGinnis and Elimelech, 2007; Mi and Elimelech, 2010; Gu et al., 2013; McGovern and Lienhard, 2014; Shaffer et al., 2015; Tow and Lienhard, 2016; Siddiqui et al., 2018). Nevertheless, similar to other membrane processes, membrane fouling remains a major obstacle hindering a wider application of FO to complex waste streams, and its combined bioreactor (e.g., osmotic membrane bioreactor (OMBR) and anaerobic membrane bioreactor (AnOMBR)) in wastewater treatment and reclamation (Mi and Elimelech, 2010; She et al., 2016; Wang et al., 2016a, 2017, 2018a, 2019; Luo et al., 2017).

Fouling occurs when solutes or particles in the feed deposit onto surfaces or into pores of the FO membrane (Liu and Mi, 2012), which not only enhances the resistance of FO membrane but also increases the external concentration polarization (ECP) (Wang et al., 2014; Motsa et al., 2015). FO membrane fouling can be classified as organic, inorganic, microbial (biofouling) and colloidal fouling (Liu and Mi, 2012; Wang et al., 2014; Sun et al., 2016). Abundant and ubiquitous organic substances in the feed water such as, natural organic matters, alginates, and proteins, induce severe fouling on FO membrane surface (Mi and Elimelech, 2008, 2010; Xie et al., 2013). In addition,

67   inorganic species not only tend to directly precipitate onto the FO membrane surface but also

68   interact with the organic foulants by bridging negatively charged functional groups (Sobeck and

69   Higgins, 2002; Boo et al., 2012). Moreover, microorganisms especially bacteria can adhere to the

70   FO membrane and subsequently form a biofilm (Yoon et al., 2013; Kwan et al., 2015), and colloidal

71   fouling is owing to the deposition of colloidal particles (Liu and Mi, 2012). Correspondingly, FO

72   membrane fouling has been extensively investigated using single model foulant such as alginate,

73   bovine serum albumin (BSA), gypsum and *Pseudomonas* aeruginosa (Mi and Elimelech, 2008;

74   Arkhangelsky et al., 2012; Kwan et al., 2015). Compared with other fouling types, organic fouling

75   is more complicated, not only because specific interactions between chemical functional groups on

76   the FO membrane surface and those of the organic foulants may occur, but it was also found to be

77   affected by the ionic composition of the feed solution (Li and Elimelech, 2006). As a result, previous

78   studies on FO membrane fouling are focused on organic fouling (Li and Elimelech, 2006; Mi and

79   Elimelech, 2010; Liu and Mi, 2012; Motsa et al., 2015; Zheng et al., 2018). In these studies, it has

80   been demonstrated that organic fouling of FO membrane is enhanced by divalent cations, i.e.,

81   forming a dense, cross-linked organic fouling layer, and consequently resulting in a rapid flux

82   decline (Li and Elimelech, 2006). It is hypothesized that if the divalent cations can be extracted

83   from the foulants on the FO membrane surface, the organic fouling layer might become loose and

84   subsequently easily remove by a simply physical cleaning.

85   Diffusive gradients in thin-films (DGT) has become an attractive technology with a wide range

86   of applications, including water quality monitoring, dynamic processes and bioavailability in waters

87   and soils (Perez et al., 2009; Town et al., 2009; Schintu et al., 2010). The DGT technology can be

88   used to adsorb most metals (e.g., Al, Zn, Cu) in water and soil based on Fick's first law of diffusion

89 (Zhang and Davison, 1995; Degryse et al., 2009; Guan et al., 2015). It consists of the innermost

90 resin layer, a specific thickness of the diffusion gel, and a membrane filter (Zhang et al., 1998; Guan

91 et al., 2015). The diffusive gel provides a controlled medium through which ions migrate before

92 being adsorbed on the resin, and the resin layer is used to absorb the enriched target ions (Sherwood

93 et al., 2009). The adsorbent material in the resin layer has a strong binding ability to metal (metalloid)

94 ions, and its target in the solution is adsorbed immediately after passing through the diffusion gel to

95 the resin layer (Davison and Zhang, 2012). The DGT technology has the advantages of simplicity,

96 *in situ* and quantitative concentration of metals and non-metallic elements, as well as morphological

97 analysis by simulating the absorption process of organisms (Zhang and Davison, 2015).

98   We are inspired by the successful extraction of metal ions from soils/sediments using DGT,

99 where the metal ions in soils/sediments are effectively transferred to the DGT and subsequently to

100 the liquid phase. In this study, applying the DGT technology for *in situ* adsorbing the divalent

101 cations binding with the organic foulants from the FO membrane surface was attempted, thereby

102 for mitigating membrane fouling and facilitating the subsequent membrane cleaning. Studies on

103 applying the DGT technology for controlling organic fouling of FO membrane were rare in current

104 literature. The objective of this study is to evaluate the feasibility of alleviating the FO membrane

105 fouling through *in situ* removing the Ca^{2+} combined with the organic foulants by the DGT

106 technology.

107 **2.   Materials and methods**

108 *2.1 Experimental set-up*

109   Fouling profile of the FO membrane was evaluated in a bench-scale filtration system, as

110 schematically shown in Fig. S1, Supporting Information. This test system included a cross-flow

111   membrane cell with two symmetric flow channels (each of 85 mm × 39 mm × 2 mm in dimension).

112   Membrane coupons were placed in the membrane cell between the two channels for the DS and FS,

113   respectively. Two peristaltic pumps (Longer Precision Pump, China) were used to pump the DS and

114   FS into the separate closed loops. The cross-flow velocity in both channels of the membrane cell

115   was constant at 1.3 mm/s. Both DS and FS were kept at room temperature (25 ± 2 ℃). Change in

116   the weight of FS was monitored by a digital balance (Mettler Toledo, China) and recorded in a

117   computer by a data acquisition software (Mettler Toledo, China), which was converted into changes

118   in water flux of FO membrane.

119   *2.2 Operating conditions*

120   Thin film composite (TFC) polyamide FO membrane (supplied by Hydration Technology

121   Innovations) was used in this study. The TFC membrane has an asymmetric structure including a

122   dense active layer (AL) and a porous support layer (SL) embedded with a polyester mesh. The water

123   permeability coefficients (*A*) and salt permeability coefficients (*B*) of the TFC FO membrane were

124   4.9×10^{12} m/(s Pa) and 0.95×10^{-7} m/s, respectively. Membrane samples were stored in deionized

125   (DI) water at 4 ℃ and soaked in DI water at room temperature for 24 h before each test.

126   A 4 M NaCl solution was used as the DS in both fouling and baseline experiments. Sodium

127   alginate (75-100 kDa) was selected as the model organic foulant. The baseline experiment was

128   conducted before the fouling experiment with the DI water as the FS and the 4 M NaCl as the DS.

129   In order to evaluate the adsorption efficiency of DGT for Ca^{2+} binding with the sodium alginate, the

130   FO membrane was fouled by the sodium alginate and $CaCl_2$ in sequence, which was different from

131   the previous fouling protocol (Liu and Mi, 2012; Motsa et al., 2015). The procedure of the FO

132   membrane fouling tests was conducted as follows (see for Fig. S2, Supporting Information). Firstly,

133 a new FO membrane coupon was sealed in the FO cell with active layer facing FS, and then a

134 baseline experiment was performed for 4 h to obtain the initial flux of the FO membrane. After that,

135 the fouling tests were started with 2 L of FS and DS. With regard to the single organic fouling, the

136 fouling filtration was operated for 48 h; while the enhanced organic fouling filtration was conducted

137 with a $CaCl_2$ solution for 24 h after the single organic fouling experiments operated for 24 h. As for

138 the single organic fouling, the FS consisted of 200 mg/L sodium alginate, 20 mM NaCl, 20 mM

139 Na_2SO_4 and 1 mM $NaHCO_3$, while the FS was changed into the $CaCl_2$ solution with three

140 concentration levels of 1, 15 and 35 mM, respectively, for the tests of enhanced organic fouling by

141 the Ca^{2+}. All the chemicals were obtained from Sigma-Aldrich (Shanghai, China).

142 *2.3 DGT adsorption and evaluation*

143 The DGT adsorption experiments were conducted after the fouling tests. As schematically

144 shown in Fig. 1, the DGT device included the membrane filter, the diffusive gel strip and the resin

145 layer (DGT Research Ltd., UK). During the adsorption experiments, the fouled FO membranes were

146 attached to the membrane filter for 48 h. After that, the resin layer made of Chelex-100 strip (a

147 commonly used chelating resin) was removed into the 1 M HNO_3 eluent for 24 h. Meanwhile, the

148 remaining foulants were removed from the FO membrane surface by ultrasound (35 Hz，15 min)

149 (Pendashteh et al., 2011). The extracted and ultrasound-extractable remaining Ca^{2+} concentrations

150 were measured by an Atomic Absorption Spectrometer (Shimadzu Tokyo, Japan).

151 Fig. 1

152 In order to evaluate the adsorption efficiency of the DGT, the extracted Ca^{2+} concentration was

153 converted into the adsorption amount on the Chelex gel strip according to the below equation.

154 $M = C_e V_e / f_e$ (1)

155 where M is the amount of Ca^{2+} absorbed on the Chelex gel strip, C_e is the concentration of Ca^{2+} in

156 the eluent, V_e is the volume of the eluent (50 mL in this study), and f_e is the elution efficiency (0.8

157 for Ca^{2+}) (Zhang and Davison, 1995; Warnken et al., 2006; Montero et al., 2012).

158   The ultrasound-extractable remaining Ca^{2+} amount on the fouled FO membrane was

159 correspondingly converted by the following equation.

160     $M_R = C_R V_R$ (2)

161   where M_R is the amount of Ca^{2+} remained on the fouled membrane surface, C_R is the

162 concentration of the ultrasound-extractable remaining Ca^{2+}, and V_R is the volume of the dissolved

163 residual foulants (100 mL in this study).

164   Based on the calculation of M and M_R, the adsorption efficiency (η) was obtained according to

165 the below equation.

166     $\eta\,(\%) = M/(M+M_R) \times 100\%$ (3)

167 *2.4 Analytical method*

168   Water flux through the FO membrane was obtained based on the weight change of the FS.

169 After the fouling tests and the DGT adsorption experiments, the water flux of the fouled and

170 adsorbed FO membranes were determined by the FO cell for 4 h with the DI water as the FS and

171 the 4 M NaCl as the DS. In order to eliminate the impacts of initial water flux (also measured by

172 the FO cell) for different FO membranes, a normalized water flux was used for characterizing the

173 fouled and adsorbed FO membranes. It was obtained through the determining flux dividing by the

174 initial flux before fouling tests.

175   The conductivity of the FS was monitored and recorded by a conductivity meter (EC300A,

176 YSI, USA). The FO membrane samples were obtained by randomly cutting from the fouled FO

177   membranes removed from the FO cell. An energy diffusive X-ray (EDX) analyzer (Su-8020, Hitachi,

178   Japan) and a field-emission scanning electron microscopy (FE-SEM) (Su-8020, Hitachi, Japan)

179   were applied for capturing the element compositions and surface images of the fouled and adsorbed

180   FO membrane samples, respectively. Prior to SEM and EDX observations, all FO membrane

181   samples were prepared by freezing the membrane at -80 $^{\circ}$C in a chiller for 2 h followed by freeze

182   drying at -48 $^{\circ}$C for 6 h using a freeze dryer (FreeZone 25, Labconco, Czech Republic). The

183   distributions of polysaccharides on the fouled and adsorbed FO membrane samples were analyzed

184   by the confocal laser scanning microscopy (CLSM) (LSM 710, ZEISS, Germany). The probe of

185   Calcofluor white (CW) (0.3 g/L) was used to stain the polysaccharides on the FO membrane samples.

186   After the labeling process, the samples were incubated for 30 min at room temperature in the dark,

187   and then were washed twice with phosphate buffered saline (PBS) solution to remove the extra

188   probes. The stained FO membrane samples were characterized by the CLSM at the

189   excitation/emission wavelengths of 405 nm/410-480 nm. Three-dimensional reconstructions were

190   obtained with ZEISS confocal software (ZEN 2012), and the images were analyzed by softwares of

191   PHLIP (Version 0.7) and Image J (NIH, Bethesda, MD, USA) to calculate the quantitative

192   parameters including average amount of polysaccharide, mean thickness and porosity (Mueller et

193   al., 2006; Yu et al., 2011; Yuan et al., 2015; Wang, et al., 2016b).

194   All experiments are repeated at least three times for statistics. The data shown in tables and

195   figures is expressed as means with standard deviations.

196   **3.   Results and discussion**

197   *3.1 Water flux profile*

198   Water flux profiles of FO membranes at different fouling conditions are shown in Fig. 2. Water

199   flux of FO membrane decreased with the extension of the operating time regardless of the

200   composition of the FS. However, the profile for FO membrane water flux decline was highly

201   dependent on the foulants composition in the FS. Compared with the single organic fouling only

202   induced by the sodium alginate, the flux decline became severer when the Ca^{2+} was added into the

203   FS. In addition, the rate for water flux decline was accelerated with an increase of the Ca^{2+}

204   concentration. Moreover, the cleaning experiments on the fouled FO membranes at different fouling

205   conditions were conducted by the backwashing in the FO cell for 0.5 h with the 0.5 M NaCl as the

206   FS and the DI water as the DS according to previous literatures (Mi and Elimelech, 2010; Motsa et

207   al., 2017) . The results indicated that the alginate fouling became difficult to clean when Ca^{2+} was

208   present in the influent, e.g., the increasing rate of the normalized water flux was about 20% for the

209   single organic fouling only induced by the sodium alginate while it became less than 5% for the

210   organic fouling induced by the sodium alginate and 35 mM Ca^{2+}. These facts clearly showed that

211   Ca^{2+} aggravated the organic fouling of FO membrane, which was consistent with previous literature

212   (Liu and Mi, 2012; Motsa et al., 2015; Charfi, et al., 2017). This phenomenon could be attributed to

213   the fact that Ca^{2+} and alginate form complexes with unique structure, thereby leading to a high

214   density gel network (Van den Brink et al., 2009; Wang and Waite, 2009).

215   Fig. 2

216   *3.2 DGT approach effectively extracted calcium from fouling layer*

217   After the fouling tests of the FO membranes, Ca^{2+} was extracted from the fouled FO

218   membranes by the DGT technology. The normalized membrane flux of the fouled FO membranes

219   before and after DGT adsorptions are summarized in Fig. 3 (a). Specifically, there were no changes

220   in the normalized water flux of the fouled FO membrane with only alginate sodium before and after

221   the DGT adsorption, indicating that the DGT had no impacts on the single organic fouling of FO

222   membrane. By contrast, the normalized water flux had a significant increase after the DGT

223   adsorption for the organic fouling enhanced by Ca^{2+}, suggesting an effective mitigation of FO

224   membrane fouling. Variations of the normalized water flux for different fouling conditions were

225   consistent with the DGT adsorption efficiency (see for Fig. 3 (b)): indeed, there was no Ca^{2+}

226   adsorption for the single organic fouling while the DGT adsorption efficiency was ranged from 32.6%

227   to 62.8% for the enhanced organic fouling with different concentrations of Ca^{2+}. These results

228   implied that the DGT could effectively adsorb Ca^{2+} from the alginate bound foulants. As a result,

229   organic fouling of the FO membrane could be alleviated via the extraction of Ca^{2+} from the fouling

230   layer.

231   Fig. 3

232   Although the DGT could adsorb the Ca^{2+} from the fouling layer of the FO membrane, the

233   adsorption amount and efficiency were significantly influenced by adding concentration of Ca^{2+}.

234   DGT adsorption amount of Ca^{2+} correspondingly increased with the feed Ca^{2+} concentration (Fig.

235   3 (b)), which was driven by more Ca^{2+} binding with the alginate at a higher addition of Ca^{2+}.

236   However, the adsorption efficiency was enhanced from 1 to 15 mM Ca^{2+}, and started to decrease

237   when Ca^{2+} concentration reached 35 mM. Given that the DGT was constrained by adsorption

238   capacity, the decrease of adsorption efficiency at Ca^{2+} concentration of 35 mM could be attributed

239   to the saturation of DGT adsorption (0.59 ± 0.01 mg). Indeed, it was interesting that the DGT

240   adsorption efficiency was not correlated with the increase of the normalized water flux after the

241   DGT adsorption (Fig. 3 (a)), suggesting that the different structure and composition of the fouling

242   layer on the FO membrane surface at different fouling conditions might strongly affect the

243   mitigation of membrane fouling by the DGT adsorption. Thus, it is very necessary to further

244   investigate the changes in structure and composition of the fouling layer before and after the DGT

245   adsorption.

246   *3.3 DGT adsorption altered fouling layer structure and improved cleaning efficiency*

247   In order to evaluate the structure of fouling layer before and after DGT adsorption, the

248   morphology, element composition and structure of fouled and DGT adsorbed FO membranes were

249   analyzed by SEM, EDX and CLSM, respectively. The SEM images of the fouled FO membranes

250   before and after the DGT adsorption are shown in Fig. 4. Compared with the SEM image of the

251   virgin FO membrane (Fig. S3), a fouling layer was formed on the FO membrane surface when only

252   sodium alginate was used. However, except for the fouling layer, some macromolecular

253   biopolymers were appeared on the FO membrane surface in all scenarios with Ca^{2+} addition into the

254   feed. More importantly, more macromolecular biopolymers deposited on the membrane surface

255   with the increase of Ca^{2+} concentration. This result further demonstrated that Ca^{2+} enhanced the

256   organic fouling and induced a severer FO membrane fouling. Noting that the high density "egg-

257   box-shaped" gel networks were observed on the FO membrane surface when Ca^{2+} concentration

258   increased to 35 mM. Correlation of foulant deposition amount on the FO membrane surface and the

259   Ca^{2+} concentration observed from SEM images were consistent with the variations of the flux

260   decline (Fig. 2). After the DGT adsorption, except for the single organic fouling induced by the

261   sodium alginate (Fig. 4 (Aa) and Fig. 4 (Ba)), the deposition of alginate fouling layer on the FO

262   membrane surface minimized regardless of the Ca^{2+} concentration, indicating the effective

263   adsorption of Ca^{2+} from the fouling layer of the FO membrane by the DGT technology.

264   Fig. 4

265   From the EDX analyses, various elements including C, O, Na, S, Cl and Ca could be detected

266   on the fouled FO membranes (Fig. S4 and Table S1). It was notable that the relative weight

267   percentage of Ca on the fouled FO membranes correspondingly increased with the increase of the

268   adding Ca^{2+} concentration, further indicating the occurrence of more severe "egg-box-shaped" gel

269   networks on the FO membrane surfaces. After the DGT adsorptions, the relative weight percentage

270   of Ca significantly reduced (Fig. S5 and Table S2). This result strongly proved the effective

271   adsorption of Ca^{2+} from the fouling layer of the FO membrane by the DGT technology.

272   For further understanding the impacts of the DGT adsorption on the fouling structure of the FO

273   membrane, the fouled FO membranes before and after the DGT adsorption were analyzed by the

274   CLSM observations. From Fig. S6, all the fouled FO membrane surfaces were covered by

275   polysaccharides, and these formed fouling layers were thick. The deposited polysaccharides slightly

276   decreased for the fouling by both sodium alginate and Ca^{2+} after the DGT adsorption (Fig. S6 and

277   Table 1). In addition, the porosity of the fouling layers induced by both the sodium alginate and

278   Ca^{2+} significantly increased after the DGT adsorption (see for Table1). It has been demonstrated

279   that the porosity significantly affects membrane fouling, i.e., less porosity results in a severe

280   membrane fouling (Wu et al., 2009; Wang et al., 2018b). Thus, the mitigation of the fouling owing

281   to both the alginate and Ca^{2+} by the DGT technology was mainly attributed to the fact that the

282   structure of the fouling layer became more porous after the extraction of the organic-bound Ca^{2+}.

283   In order to further investigate whether DGT adsorption could enhance the physical cleaning,

284   the fouled and DGT adsorbed FO membranes at the FS condition of sodium alginate and 35 mM

285   Ca^{2+} were backwashed according to previous literature (Mi and Elimelech, 2010; Motsa et al., 2017).

286   There was no significant variation of the normalized water flux for the fouled FO membrane after

287 the backwashing; by contrast, it significantly increased from 0.41 to 0.53 for the DGT adsorbed FO

288 membrane after backwashing (Fig. 5). It suggested that the DGT adsorption could enhance the

289 physical cleaning of the fouled FO membranes. Such evidence strongly suggested that the DGT

290 adsorption not only mitigated the FO membrane fouling but also enhanced the membrane cleaning

291 via changing the structure of the fouling layer.

292 Fig. 5

293 *3.4 Implications*

294 We demonstrated that the DGT technology can effectively alleviate organic fouling of FO

295 membranes via directly adsorbing Ca^{2+} from the fouling layer. The mechanisms on the *in situ*

296 mitigating FO membrane fouling are conceptualized in Fig. 6. With regard to a thick fouling layer

297 with alginate-Ca^{2+} gel networks, the Chelex resin in the DGT device can directly remove the

298 alginate-bound Ca^{2+} via the chelation of the Chelex functional groups. Due to the extraction of the

299 alginate-bound Ca^{2+} from the organic fouling layer, the structure of the fouling layer became more

300 porous and looser, which mitigated the FO membrane fouling and further enhanced the cleaning

301 efficiency. Moreover, the DGT devise can be reused for adsorbing Ca^{2+} after the resin layer was

302 regenerated by HNO_3 based on the results that the reused DGT device had a similar Ca^{2+} adsorption

303 amount compared with the new one. The success in alleviating organic fouling of the FO membrane

304 demonstrated the feasibility of fouling control strategy via directly extracting Ca^{2+} from the fouling

305 layer. Extracting the calcium from fouling layer played a critical role in altering membrane fouling

306 layer structure, which shed light on novel fouling control and management. However, applying such

307 DGT-based technique in controlling real FO membrane fouling still has limitations. On one hand,

308 the real FO fouling is composed of many other constituents such as precipitates, microorganisms,

309 and humic substances, which might disrupt the extraction of Ca^{2+} from the fouling layer. On the

310 other hand, although the DGT technology was suitable for the flat-sheet FO membrane module

311 applied in this study, it is difficult to directly apply in the spiral-wound or other tightly-packed

312 membrane configurations. Thus, further studies should be focused on evaluating the DGT

313 technology in real fouling scenarios where the co-existence of sparingly soluble inorganic minerals

314 and organic foulants leads to a more complicated membrane fouling, and emphasized on developing

315 other chelating agent or resin to replace with the DGT technology for in situ adsorbing calcium from

316 the fouling layer in order to adapt to different foulants composition and membrane configurations.

317 Fig. 6

318 **4. Conclusions**

319 This study proposes a novel approach to mitigating the FO membrane fouling via the DGT for

320 *in situ* removing Ca^{2+} binding with organic foulants. With regard to a thick fouling layer with

321 alginate-Ca^{2+} gel networks, the Chelex resin in the DGT equipment can directly remove the organic-

322 bound Ca^{2+} via the chelation. Owing to the extraction of the organic-bound Ca^{2+} from the membrane

323 surface, the structure of the fouling layer became more porous and looser. The changes in the fouling

324 structure alleviated the FO membrane fouling and further enhanced the cleaning effect. The success

325 in mitigating the FO membrane fouling induced by the sodium alginate and Ca^{2+} demonstrated the

326 feasibility of fouling controlling strategy via directly extracting Ca^{2+} from the fouling layer.

334   **Appendix A. Supplementary information**

335   Detailed information on additional tables and figures can be found in the Supporting

336   Information.

337   **References**

338   Arkhangelsky, E., Wicaksana, F., Tang, C.Y., Al-Rabiah, A.A., 2012. Combined organic-inorganic

339   fouling of forward osmosis hollow fiber membranes. Water Res. 46 (19), 6329-6338.

340   Boo, C., Lee, S., Elimelech, M., Meng, Z.Y., Hong, S., 2012. Colloidal fouling in forward osmosis:

341   Role of reverse salt diffusion. J. Membr. Sci. 390-391, 277-284.

342   Charfi, A., Jang, H., Kim, J., 2017. Membrane fouling by sodium alginate in high salinity conditions

343   to simulate biofouling during seawater desalination. Bioresour. Technol. 240, 106-114.

344   Davison, W., Zhang, H., 2012. Progress in understanding the use of diffusive gradients in thin films

345   (DGT) - back to basics. Environ. Chem. 9 (1), 1-13.

346   Degryse, F., Smolders, E., Zhang, H., Davison, W., 2009. Predicting availability of mineral

347   elements to plants with the DGT technique: a review of experimental data and interpretation

348   by modelling. Environ. Chem. 6 (3), 198-218.

349   Gu, Y.S., Wang, Y.N., Wei, J., Tang, C.Y., 2013. Organic fouling of thin-film composite polyamide

350   and cellulose triacetate forward osmosis membranes by oppositely charged macromolecules.

351   Water Res. 47, 1687-1874.

352   Guan, D.X., Williams, P.N., Luo, J., Zheng, J.L., Xu, H.C., Cai, C., Ma, L.N.Q., 2015. Novel

353   precipitated zirconia-based DGT technique for high-resolution imaging of oxyanions in waters

354   and sediments. Environ. Sci. Technol. 49 (6), 3653-3661.

355   Kwan, S.E., Bar-Zeev, E., Elimelech, M., 2015. Biofouling in forward osmosis and reverse osmosis:

356   Measurements and mechanisms. J. Membr. Sci. 493, 703-708.

357   Li, Q.L., Elimelech, M., 2006. Synergistic effects in combined fouling of a loose nanofiltration

358   membrane by colloidal materials and natural organic matter. J. Membr. Sci. 278 (1), 72-82.

359   Liu, Y.L., Mi, B.X., 2012. Combined fouling of forward osmosis membranes: Synergistic foulant

360   interaction and direct observation of fouling layer formation. J. Membr. Sci. 407-408, 136-144.

361   Luo, W.H., Phan, H.V., Xie, M., Hai, F.I., Price, W.E., Elimelech, M., Nghiem, L.D., 2017. Osmotic

362   versus conventional membrane bioreactors integrated with reverse osmosis for water reuse:

363   Biological stability, membrane fouling, and contaminant removal. Water Res. 109, 122-134.

364   Lutchmiah, K., Verliefde, A.R.D., Roest, K., Rietveld, L.C, Cornelissen, E.R., 2014. Forward

365   osmosis for application in wastewater treatment: A review. Water Res. 58, 179-197.

366   Mi, B.X., Elimelech, M., 2008. Chemical and physical aspects of organic fouling of forward

367   osmosis membranes. J. Membr. Sci. 320, 292-302.

368   Mi, B.X., Elimelech, M., 2010. Organic fouling of forward osmosis membranes: Fouling

369   reversibility and cleaning without chemical reagents. J. Membr. Sci. 348 (1), 337-345.

370   McGinnis, R.L., Elimelech, M., 2007. Energy requirements of ammonia-carbon dioxide forward

371   osmosis desalination. Desalination 207 (1), 370-382.

372   McGovern, R.K., Lienhard, J.H., 2014. On the potential of forward osmosis to energetically

373   outperform reverse osmosis desalination. J. Membr. Sci. 469, 245-250.

374   Montero, N., Belzunce-Segarra, M.J., Gonzalez, J.L., Larreta, J., Franco, J., 2012. Evaluation of

375   diffusive gradients in thin-films (DGTs) as a monitoring tool for the assessment of the chemical

376   status of transitional waters within the Water Framework Directive. Mar. Pollut. Bull. 64 (1),

377   31-39.

378 Motsa, M.M., Mamba, B.B., Verliefde, A.R.D., 2015. Combined colloidal and organic fouling of

379   FO membranes: The influence of foulant-foulant interactions and ionic strength. J. Membr. Sci.

380   493, 539-548.

381 Motsa, M.M., Mamba, B.B., Thwala, J.M., Verliefde, A.R.D., 2017. Osmotic backwash of fouled

382   FO membranes: Cleaning mechanisms and membrane surface properties after cleaning.

383   Desalination 402, 62-71.

384 Mueller, L.N., de Brouwer, J.F.C., Almeida, J.S., Stal, L.J., Xavier, J.B., 2006. Analysis of a marine

385   phototrophic biofilm by confocal laser scanning microscopy using the new image

386   quantification software PHLIP. BMC Ecol. 6, 1-15.

387 Pendashteh, A.R., Fakhru'l-Razi, A., Madaeni, S.S., Abdullah, L.C., Abidin, Z.Z., Biak, D.R.A.,

388   2011. Membrane foulants characterization in a membrane bioreactor (MBR) treating

389   hypersaline oily wastewater. Chem. Eng. J. 168 (1), 140-150.

390 Perez, A.L., Anderson, K.A., 2009. DGT estimates cadmium accumulation in wheat and potato from

391   phosphate fertilizer applications. Sci. Total. Environ. 407 (18), 5096-5103.

392 Schintu, M., Marras, B., Durante, L., Meloni, P., Contu, A., 2010. Macroalgae and DGT as

393   indicators of available trace metals in marine coastal waters near a lead-zinc smelter. Environ.

394   Monit. Assess. 167 (1), 653-661.

395 Shaffer, D.L., Werber, J.R., Jaramillo, H., Lin, S.H, Elimelech, M., 2015. Forward osmosis: Where

396   are we now? Desalination 356, 271-284.

397   She, Q.H., Wang, R., Fane, A.G., Tang, C.Y., 2016. Membrane fouling in osmotically driven

398   membrane processes: A review. J. Membr. Sci. 499, 201-233.

399   Sherwood, J.E., Barnett, D., Barnett, N.W., Dover, K., Howitt, J., Ii, H., Kew, P., Mondon, J., 2009.

400   Deployment of DGT units in marine waters to assess the environmental risk from a deep sea

401   tailings outfall. Anal. Chim. Acta. 652 (1-2), 215-223.

402   Siddiqui, F.A., She, Q.H., Fane, A.G., Field, R.W., 2018. Exploring the differences between forward

403   osmosis and reverse osmosis fouling. J. Membr. Sci. 565, 241-253.

404   Sobeck, D.C., Higgins, M.J., 2002. Examination of three theories for mechanisms of cation-induced

405   bioflocculation. Water Res. 36, 527-538.

406   Sun, Y., Tian, J.Y., Zhao, Z.W., Shi, W.X., Liu, D.M., Cui, F.Y., 2016. Membrane fouling of

407   forward osmosis (FO) membrane for municipal wastewater treatment: A comparison between

408   direct FO and OMBR. Water Res. 104, 330-339.

409   Tow, E.W., Lienhard, J.H., 2016. Quantifying osmotic membrane fouling to enable comparisons

410   across diverse processes. J. Membr. Sci. 511, 92-107.

411   Town, R.M., Chakraborty, P., Van Leeuwen, H.P., 2009. Dynamic DGT speciation analysis and

412   applicability to natural heterogeneous complexes. Environ. Chem. 6 (2), 170-177.

413   Van den Brink, P., Zwijnenburg, A., Smith, G., Temmink, H., Van Loosdrecht, M., 2009. Effect of

414   free calcium concentration and ionic strength on alginate fouling in cross-flow membrane

415   filtration. J. Membr. Sci. 345 (1), 207-216.

416   Wang, X.M., Waite, T.D., 2009. Role of Gelling Soluble and Colloidal Microbial Products in

417   Membrane Fouling. Environ. Sci. Technol. 43 (24), 9341-9347.

418   Wang, Z.W., Ma, J.X., Tang, C.Y., Kimura, K., Wang, Q.Y., Han, X.M., 2014. Membrane cleaning

419   in membrane bioreactors: A review. J. Membr. Sci. 468, 276-307.

420   Wang, X.H., Chang, V.W.C., Tang, C.Y., 2016a. Osmotic membrane bioreactor (OMBR)

421   technology for wastewater treatment and reclamation: Advances, challenges, and prospects for

422   the future. J. Membr. Sci. 504, 113-132.

423   Wang, X.H., Zhao, Y.X., Yuan, B., Wang, Z.W., Li, X.F., Ren, Y.P., 2016b. Comparison of

424   biofouling mechanisms between cellulose triacetate (CTA) and thin-film composite (TFC)

425   polyamide forward osmosis membranes in osmotic membrane bioreactors. Bioresour. Technol.

426   202, 50-58.

427   Wang, X.H., Hu, T.Z., Wang, Z.W., Li, X.F., Ren, Y.P., 2017. Permeability recovery of fouled

428   forward osmosis membranes by chemical cleaning during a long-term operation of anaerobic

429   osmotic membrane bioreactors treating low-strength wastewater. Water Res. 123, 505-512.

430   Wang, X.H., Zhang, J.F., Chang, V.W.C., She Q.H., Tang C.Y., 2018a. Removal of cytostatic drugs

431   from wastewater by an anaerobic osmotic membrane bioreactor. Chem. Eng. J. 339, 153-161.

432   Wang, W.Y., Yue, Q.Y., Li, R.H., Bu, F., Shen, X., Gao, B.Y., 2018b. Optimization of coagulation

433   pre-treatment for alleviating ultrafiltration membrane fouling: The role of floc properties on Al

434   species. Chemosphere 200, 86-92.

435   Wang, H.L., Wang, X.H., Meng, F.G., Li, X.F., Ren, Y.P., She, Q.H., 2019. Effect of driving force

436   on the performance of anaerobic osmotic membrane bioreactors: New insight into enhancing

437   water flux of FO membrane via controlling driving force in a two-stage pattern. J. Membr. Sci.

438   569, 41-47.

439   Warnken, K.W., Zhang, H., Davison, W., 2006. Accuracy of the Diffusive Gradients in Thin-Films

440   Technique: Diffusive boundary layer and effective sampling area considerations. Anal. Chem.

441   78 (11), 3780-3787.

442   Wu, B., An, Y.Y., Li, Y.Z., Wong, F.S., 2009. Effect of adsorption/coagulation on membrane

443   fouling in microfiltration process post-treating anaerobic digestion effluent. Desalination 242

444   (1), 183-192.

445   Xie, M., Nghiem, L.D., Price, W.E., Elimelech, M., 2013. Impact of humic acid fouling on

446   membrane performance and transport of pharmaceutically active compounds in forward

447   osmosis. Water Res. 47 (13), 4567-4575.

448   Yoon, H., Baek, Y., Yu, J., Yoon, J., 2013. Biofouling occurrence process and its control in the

449   forward osmosis. Desalination 325, 30-36.

450   Yu, G.H., Tang, Z., Xu, Y.C., Shen, Q.R., 2011. Multiple fluorescence labeling and two dimensional

451   FTIR-13C NMR heterospectral correlation spectroscopy to characterize extracellular

452   polymeric substances in biofilms produced during composting. Environ. Sci. Technol. 45 (21),

453   9224-9231.

454   Yuan, B., Wang, X.H., Tang, C.Y., Li, X.F., Yu, G.H., 2015. In situ observation of the growth of

455   biofouling layer in osmotic membrane bioreactors by multiple fluorescence labeling and

456   confocal laser scanning microscopy. Water Res. 75, 188-200.

457   Zhang, H., Davison, W., 1995. Performance Characteristics of Diffusion Gradients in Thin Films

458   for the in Situ Measurement of Trace Metals in Aqueous Solution. Anal. Chem. 67 (19), 3391-

459   3400.

460   Zhang, H., Davison, W., Knight, B., McGrath, S., 1998. In Situ Measurements of Solution

461   Concentrations and Fluxes of Trace Metals in Soils Using DGT. Environ. Sci. Technol. 32 (5),

462   704-710.

463   Zhang, H., Davison, W., 2015. Use of diffusive gradients in thin-films for studies of chemical

464   speciation and bioavailability. Environ. Chem. 12 (2), 85-101.

465   Zhao, S.F., Zou, L., Tang, C.Y., Mulcahy, D., 2012. Recent developments in forward osmosis:

466   Opportunities and challenges. J. Membr. Sci. 396, 1-21.

467   Zheng, L., Price, W.E., Nghiem, L.D., 2018. Effects of fouling on separation performance by

468   forward osmosis: the role of specific organic foulants. Environ. Sci. Pollut. R. 1-12.

469

470 **Table Captions**

471 Table 1 Structural parameters of fouling layer before and after DGT adsorption obtained from

472 CLSM images via PHLIP[a].

473 **Figure Captions**

474 Fig. 1. Schematic view of the DGT adsorption device for the fouled FO membranes.

475 Fig. 2. Water flux profile of FO membranes during fouling filtration. FO fouling filtration was

476 conducted with feed solution containing 200 mg/L sodium alginate, 20 mM NaCl, 20 mM Na_2SO_4

477 and 1 mM $NaHCO_3$, with varying calcium concentration from 1 to 35 mM. Draw solution was 4 M

478 NaCl. The filtration was operated for 24 hours.

479 Fig. 3. DGT performance in fouling mitigation: (A) Normalized water flux and (B) DGT adsorption

480 amount and efficiency at different fouling conditions. The FO fouling filtration conditions were

481 described in Figure 2. DGT adsorption was performed using a DGT device with Chelex-100 strip,

482 1 M HNO_3 as the eluent. The error bar represents the standard deviation from three repeated

483 experiments.

484 Fig. 4. SEM images of the fouled (A) and DGT adsorbed (B) FO membranes: (a) single organic

485 fouling; (b) organic fouling + 1 mM Ca^{2+}; (c) organic fouling + 15 mM Ca^{2+}; (d) organic fouling +

486 35 mM Ca^{2+}.

487 Fig. 5. CLSM images of the fouled (A) and DGT adsorbed (B) FO membranes with alginate and 35

488 mM Ca^{2+} and normalized water flux before and after backwashing (C). Experimental condition for

489 FO filtration was described in Figure 2, and DGT adsorption protocol was described in Figure 3.

490 Fig. 6. Mechanisms of Ca^{2+} adsorption from the fouling layer by the DGT technology.

491

492   Table 1 Structural parameters of fouling layer before and after DGT adsorption obtained

493   from CLSM images via PHLIP[a].

	Fouling layer	Average amount of polysaccharide ($\mu m^3\ \mu m^{-2}$)	Porosity (%)	Mean thickness (μm)
	single organic fouling	12.25 ± 0.41	32.10 ± 4.70	24.85 ± 1.32
Before DGT adsorption	organic fouling + 1 mM Ca^{2+}	13.00 ± 1.08	22.78 ± 7.54	24.81 ± 3.69
	organic fouling + 15 mM Ca^{2+}	14.06 ± 0.93	18.26 ± 9.46	26.26 ± 1.44
	organic fouling + 35 mM Ca^{2+}	14.13 ± 0.87	16.27 ± 0.80	25.56 ± 3.38
	single organic fouling	12.45 ± 0.05	35.06 ± 2.51	24.68 ± 3.26
After DGT adsorption	organic fouling + 1 mM Ca^{2+}	12.40 ± 0.09	33.49 ± 2.90	22.31 ± 0.95
	organic fouling + 15 mM Ca^{2+}	13.00 ± 0.19	28.14 ± 8.81	23.46 ± 0.29
	organic fouling + 35 mM Ca^{2+}	13.14 ± 0.26	20.86 ± 3.62	24.78 ± 0.49

494   [a] Values are given as mean values ± standard deviation (number of measurements: n=3). The

495   scanning area was $850 \times 850\ \mu m^2$ in size.

496

497

498

499

500

501

502
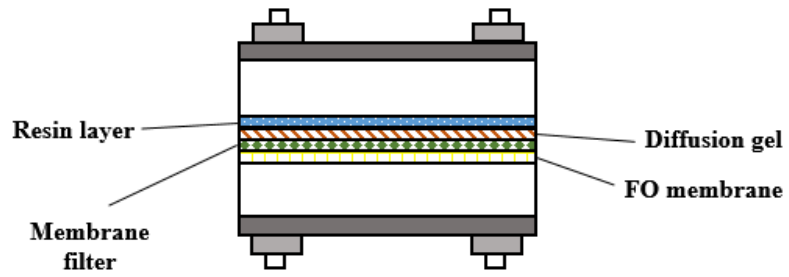
503

504   Fig. 1. Schematic view of the DGT adsorption device for the fouled FO membranes.

505

506
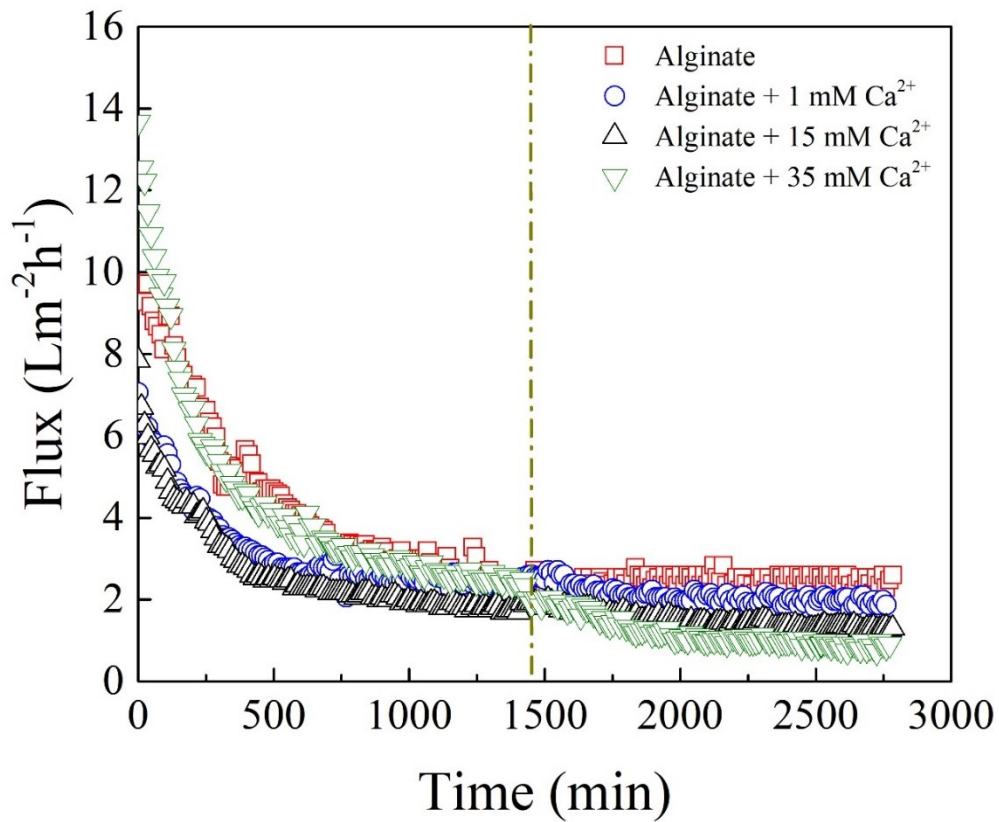
507

508

509

510

511

512

513

514

515

516

517

518

519

520

521

Fig. 2. Water flux profile of FO membranes during fouling filtration. FO fouling filtration was conducted with feed solution containing 200 mg/L sodium alginate, 20 mM NaCl, 20 mM Na_2SO_4 and 1 mM $NaHCO_3$, with varying calcium concentration from 1 to 35 mM. Draw solution was 4 M NaCl. The filtration was operated for 24 hours.

535
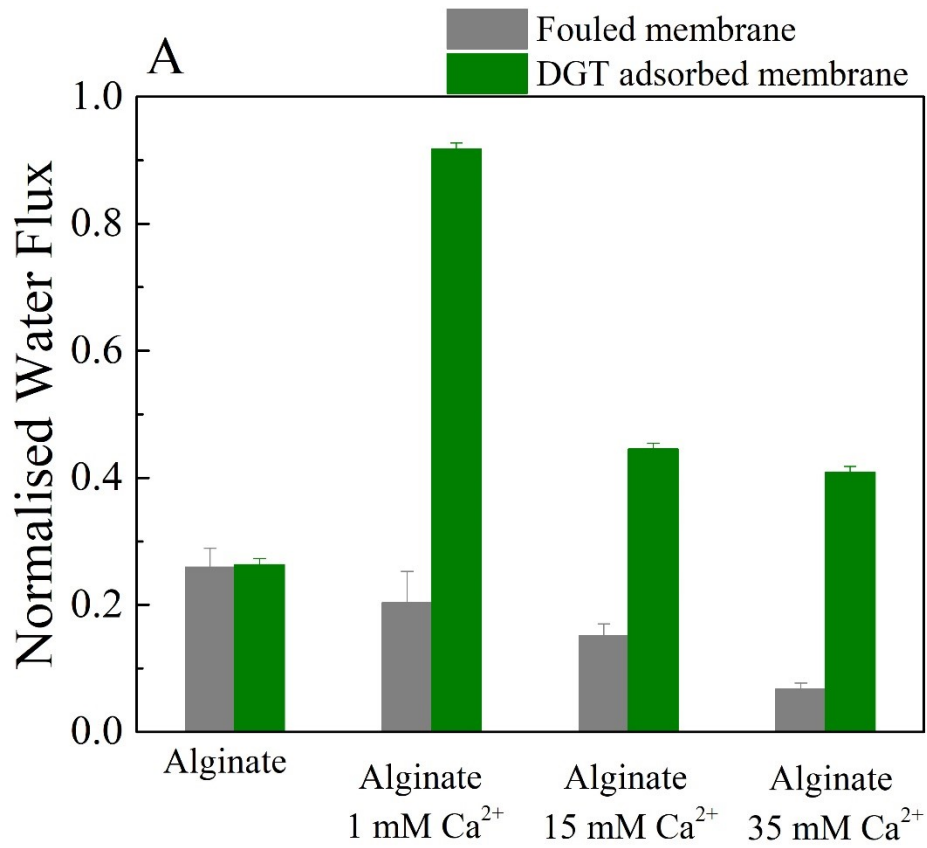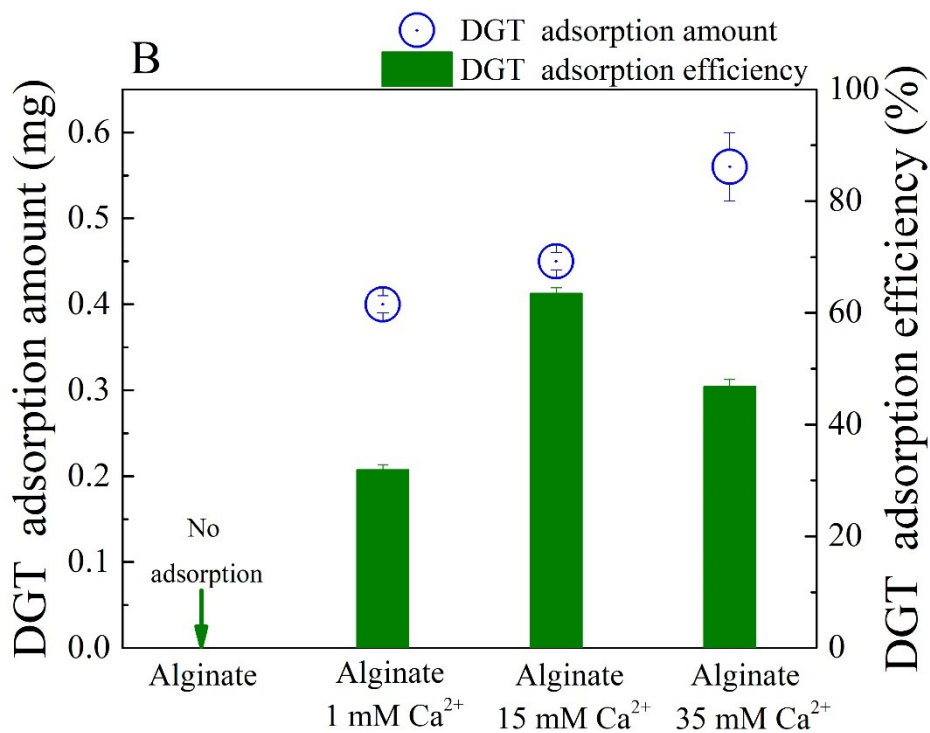
536

537

Fig. 3. DGT performance in fouling mitigation: (A) Normalized water flux and (B) DGT

adsorption amount and efficiency at different fouling conditions. The FO fouling filtration

540   conditions were described in Figure 2. DGT adsorption was performed using a DGT device with

541   Chelex-100 strip, 1 M HNO_3 as the eluent. The error bar represents the standard deviation from

542   three repeated experiments.

543

544

545

546

547

548

549

550

551

552

553

554

555
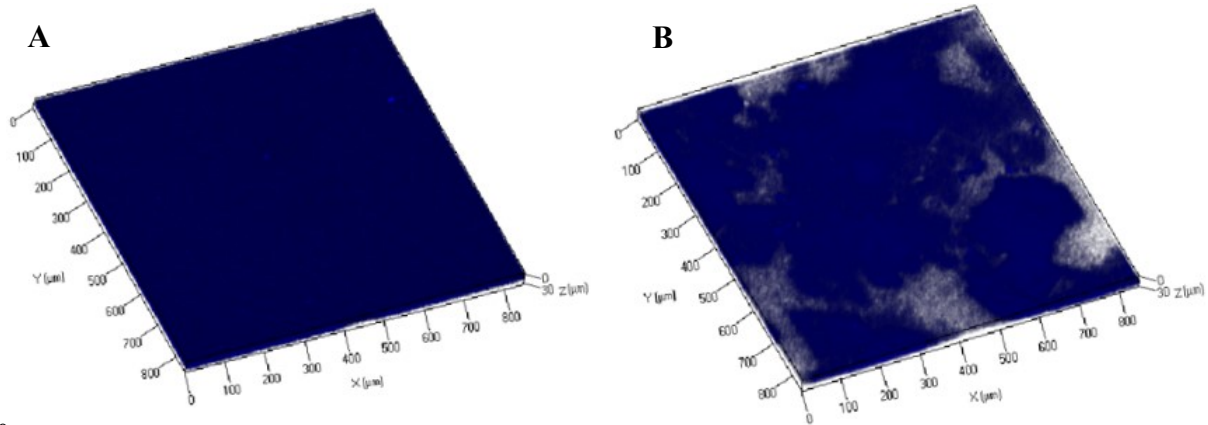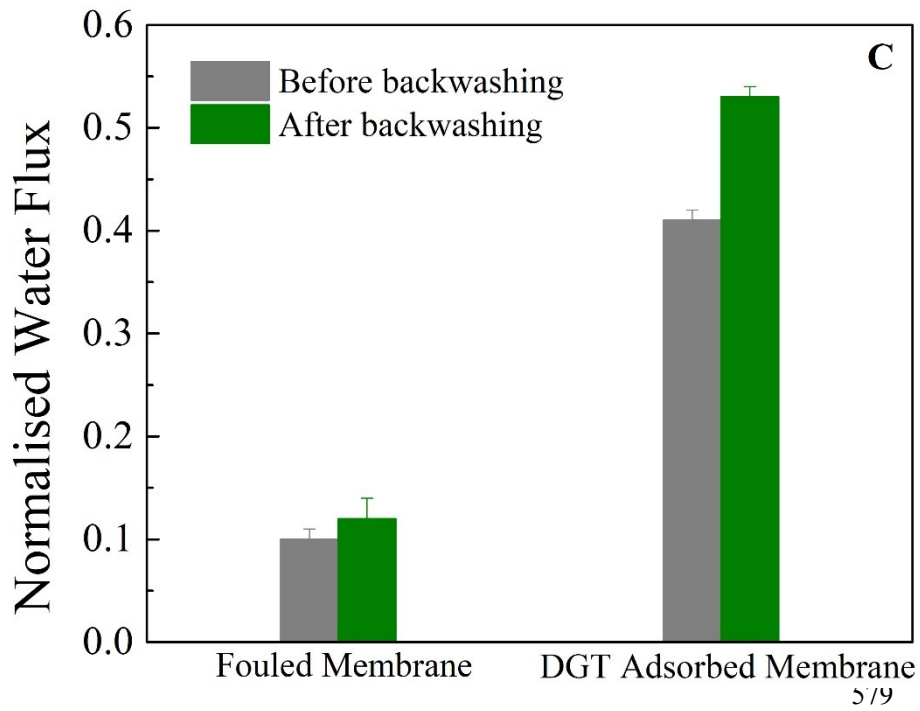
556

557

558

559

560

561

562

563

564

565
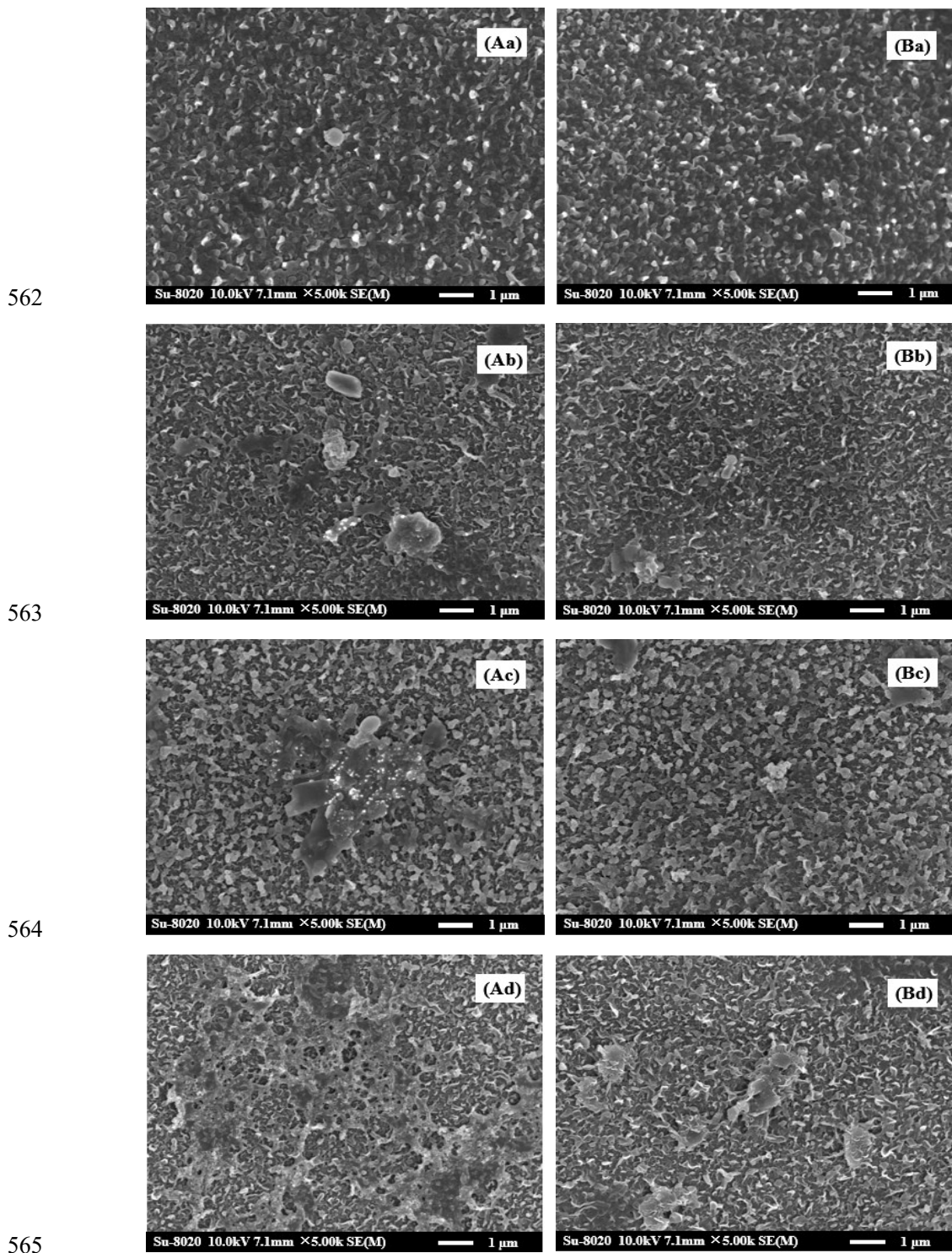
Fig. 4. SEM images of the fouled (A) and DGT adsorbed (B) FO membranes: (a) single organic

fouling; (b) organic fouling + 1 mM Ca^{2+}; (c) organic fouling + 15 mM Ca^{2+}; (d) organic fouling +
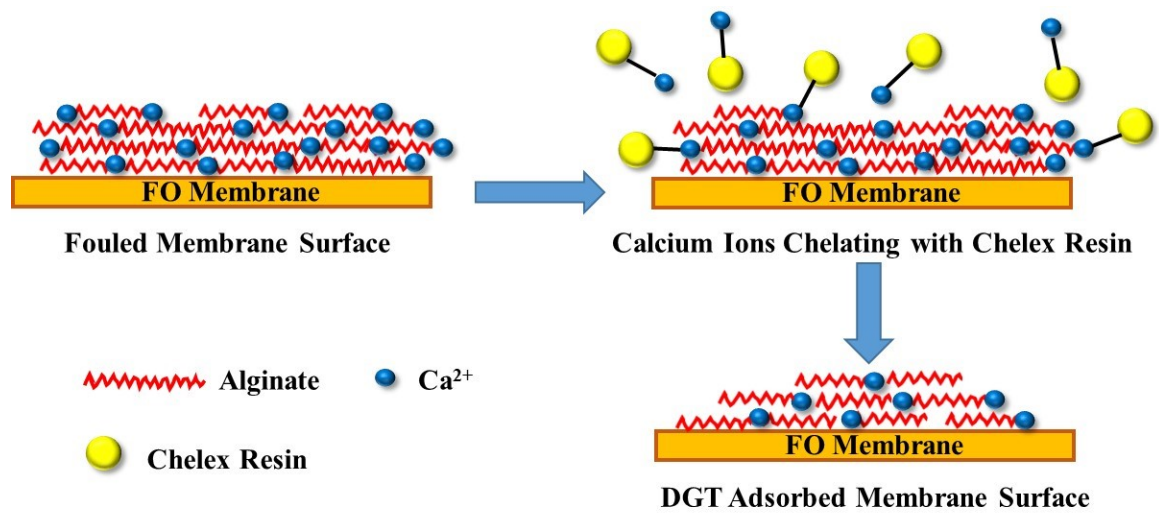
35 mM Ca^{2+}.

569

570

579

580   Fig. 5. CLSM images of the fouled (A) and DGT adsorbed (B) FO membranes with alginate and

581   35 mM Ca^{2+} and normalized water flux before and after backwashing (C). Experimental condition

582   for FO filtration was described in Figure 2, and DGT adsorption protocol was described in Figure

583   3.

584

585

586

587

588   Fig. 6. Mechanisms of Ca^{2+} adsorption from the fouling layer by the DGT technology.